JOURNAL OF GEOPHYSICAL RESEARCH, VOL. 114, C09019, doi:10.1029/2007JC004660, 2009

Intensified upwelling over a widened shelf in the northeastern South China Sea

Jianping Gan,[1] Anson Cheung,[1] Xiaogang Guo,[2] and Li Li[2]

Received 24 November 2007; revised 24 May 2009; accepted 18 June 2009; published 23 September 2009.

[1] Observational and three-dimensional modeling studies reveal that the intensified upwelling in the northeastern South China Sea (NSCS) is formed as a result of intensified upslope advection of dense deep waters that cross the middle shelf toward the inner shelf over a distinctly eastward widened shelf. The strongest advection occurs over the converging isobaths near the head of the widened shelf. As these dense deep waters advance shoreward, they are advected downstream by the quickly developed upwelling current over the inner shelf and eventually outcropped at the lee of a coastal cape. Dynamically, the shoreward cross-isobath transport over the widened shelf is geostrophically enhanced by a quasi-barotropic negative (westward) along-isobath pressure gradient force as a result of the net rate of the momentum influx and by an intensified bottom frictional transport owing to the flow confluence near the head of the widened shelf. A negative pressure gradient also exists at the lee of the coastal cape over the inner shelf and locally amplifies shoreward motion. Induced by the respective widened shelf and the coastal promontory, the along-isobath variations of cross-isobath transport in the water column over the middle and inner shelves interactively characterize intensified upwelling in the NSCS.

Citation: Gan, J., A. Cheung, X. Guo, and L. Li (2009), Intensified upwelling over a widened shelf in the northeastern South China Sea, *J. Geophys. Res.*, *114*, C09019, doi:10.1029/2007JC004660.

1. Introduction

[2] In wind-driven coastal upwelling, the alongshore variation of the shelf topography largely constrains the orientation of the alongshore flow and geostrophically modulates the intensity of the cross-shelf transport [*Gan and Allen*, 2002]. The cross-shelf gradient of isobaths over the continental shelf, on the other hand, controls the intensity of the upwelling jet and the ensuing cross-shelf bottom frictional transport [*Allen et al.*, 1995; *Weisberg et al.*, 2005]. The upward motion over the nearshore waters in the upwelling is regulated not only by the characteristics of the topography over the inner shelf, but also by those over the middle and outer shelves [*Weisberg et al.*, 2005]. The variable shelf topography, in both along-shelf and across-shelf directions, markedly controls the shoreward advection of denser deep water by virtue of the bottom Ekman transport and geostrophy. The combined topographic influence from nearshore and farther offshore regions is expected to interact each other and control the path and intensity of the coastal current, the shoreward transport and the associated correlation scale of the cross-shelf flow over the continental shelf. The forcing process induced by the shelf topography and exerted on the wind-driven upwelling circulation, particularly on the cross-shelf circulation that transports large gradients of physical and tracer properties upslope over a sufficiently wide shelf with variable topography, remains poorly understood. This study reports on the variations in coastal upwelling as a result of control by the shelf topography over the broad continental shelf in the northeastern South China Sea (NSCS) (Figure 1).

[3] The shelf topography in the NSCS is characterized by the complex coastline variation in the nearshore region and by the existence of a prominent eastward widened shelf (referred to as the widened shelf hereafter) formed by an abrupt offshore extension of isobaths east of the Pearl River Estuary and bounded by the 50 m isobath at its southern edge (Figure 1). A shallow bank, the Taiwan Shoals, is located between the 50 m isobath in the south and the 30 m isobath in the north at the eastern end of the widened shelf. Prominent features in the widened shelf includes the embedded capes along the coastline and shoreward convex isobaths that converge near the head of the widened shelf about half a degree southwest of Shanwei.

[4] Under the influence of the East Asian monsoon, southwesterly upwelling favorable winds prevail over the NSCS during the summer in June, July and August [*Li*, 1993]. As a result, coastal upwelling is generated along the coast of the NSCS in which cold and nutrient-rich deep waters upwell to the surface layer over the broad shelf. The upwelling in the NSCS has a strong spatial variation. The intensified upwelling (IU) is found over the widened shelf

[1]Department of Mathematics and Atmospheric, Marine and Coastal Environment Program, Hong Kong University of Science and Technology, Kowloon, Hong Kong.
[2]Third Institute of Oceanography, State Oceanic Administration, Xiamen, China.

0148-0227/09/2007JC004660$09.00

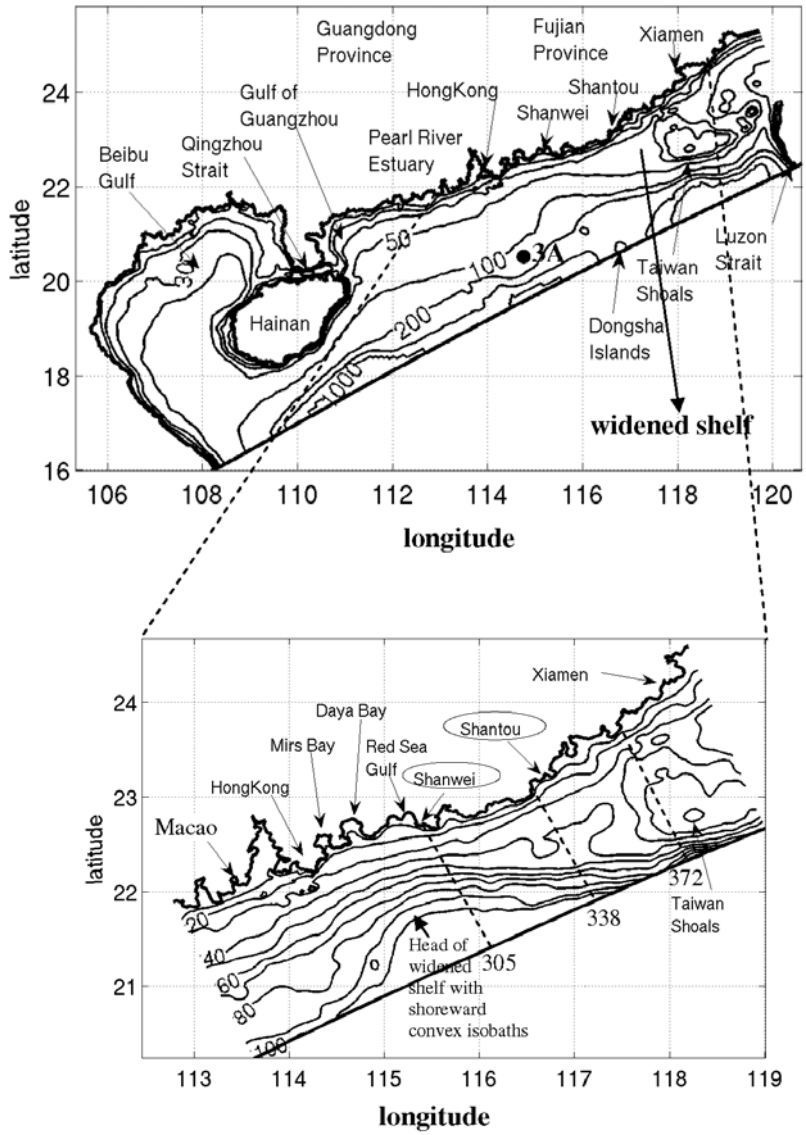

Figure 1. The topography (in meters) in the northern South China Sea and the zoomed area in the region between Guangdong and Xiamen. The selected cross-shelf sections (dashed lines) are marked by their grid numbers. The location of shoreward convex isobaths exists at the head of the widened shelf about half a degree southwest of Shanwei.

(Figures 2 and 4) with a maximum intensity at the lee of a coastal cape near Shantou (116.7°E (Figures 1 and 2)). The spatial structure of the upwelling appears to be largely correlated with the topographic characteristics of the widened shelf. Following early findings on upwelling in the NSCS [*Wyrtki*, 1961], strong upwelling centers have been identified either in Shantou by *Li* [1993] or at relatively less frequent occurrences, in Shanwei (115.5°E) by *Zeng* [1986] and *Han and Ma* [1988] from many hydrographic measurements. However, there have been few investigations that describe the basic process and the forcing mechanism of the IU in the NSCS. In particular, the effect from the unique NSCS shelf topography on the upwelling circulation has not been explored.

[5] The intensity of the coastal upwelling is governed by the strength of the wind-driven surface Ekman transport and the shoreward return currents in the interior and bottom boundary layer in a cross-shelf, two-dimensional view. For a given wind forcing, the two-dimensional upwelling is characterized to a great extent by the cross-shelf topography. In a cross-shelf, two-dimensional modeling study, *Allen et al.* [1995] showed that the coastal jet in an upwelling at a given time is stronger over a steep shelf, while the frictional bottom boundary layer develops more strongly and carries a larger fraction of the onshore Ekman transport over a wider shelf. A three-dimensional upwelling flow field can deviate substantially from the two-dimensional flow as a result of variable forcing in the alongshore direction. Besides an alongshore variation in wind forcing, the alongshore variation in the pressure gradient induced by the shelf topography [e.g., *Lentz et al.*, 1999; *Weisberg et al.*, 2005] plays a key role in forming the alongshore variation in the upwelling in many coastal regions around the world.

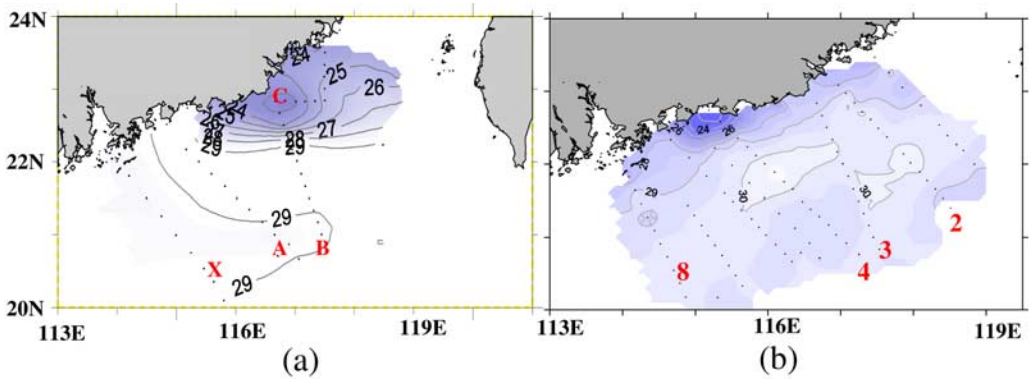

Figure 2. Water temperature (°C) at 5 m obtained from CTD transects during summer cruises (a) in 2000 and (b) in 2002. The dots are profiling locations, and the transects are marked with a number or a letter.

[6] Over a sufficiently wide shelf like in NSCS, wind-forced coastal circulation varies across the shelf with distinctive regions defined as inner, middle and outer shelf as a result of variable dynamical forcing regimes. The inner shelf is the nearshore waters of overlapping surface and bottom Ekman layers [*Mitchum and Clarke*, 1986; *Lentz*, 1995], or inshore of the upwelling front where weakly stratified or unstratified waters are located [*Austin and Lentz*, 2002]. A more comprehensive definition for the inner, middle and outer shelf was given by *Li and Weisberg* [1999a, 1999b] and *Weisberg et al.* [2005], in which the inner shelf is the transition region between the Ekman and Ekman geostrophic balances where the surface slope results from mass adjustments through overlapping surface and the bottom Ekman layer, the outer shelf is the region that extends a baroclinic Rossby radius of deformation landward from the shelf break and the middle shelf is located between them. *Weisberg et al.* [2001] also pointed out that the inner shelf can include a geostrophic interior region so long as the surface and bottom Ekman layers are connected via divergence.

[7] The upwelling over the nearshore water is controlled by the interaction of the wind-driven cross-shelf exchange over the inner, middle and/or outer shelves. The intensity of the interaction, besides other controlling factors like stratification and wind forcing, is governed by the nature of the shelf topography. In the alongshore direction, *Gan and Allen* [2002] found that a stronger upwelling occurred in the lee of a coastal promontory along the coast of California, where the cross-shelf circulation is geostrophically strengthened by a locally amplified alongshore pressure gradient. A similar response extends to the middle shelf as the scale of the topography characteristic is expanded beyond the inner shelf [*Song et al.*, 2001]. In the cross-shelf direction, *Janowitz and Pietrafesa* [1982] showed that the diverging shelf isobaths produce a variation in the vorticity and leads to the formation of a vertical vorticity as well as a cross-isobath flow. On the other hand, the accelerated along-shelf flow over the continental shelf with converging isobaths leads to an increase in the frictional bottom transport favorable to the upwelling [*Oke and Middleton*, 2000; *Weisberg et al.*, 2000]. *Pringle* [2002] used a barotropic, linear and steady potential vorticity equation, showed that the onshore transport of deep waters, primarily in the bottom layer enhances in the place where the shelf narrows down wave during upwelling. In the recent Coastal Ocean Advances in Shelf Transport (COAST) program, *Barth et al.* [2005], *Kosro* [2005] and *Gan and Allen* [2005a] showed that the intensity and the pattern of the upwelling circulation are greatly regulated by the existence of a coastal bank embedded over a relatively uniform shelf off Oregon. They found that stronger cooling was introduced by the intensified cross-shelf circulation and heat advection over the coastal bank. In spite of the obvious correlation between the coastal circulation and topographic forcing, a dynamical rationalization remains unclear. In particular, the processes and dynamics involved in the interactive response of wind-driven, cross-shelf transport over the inner and middle shelves to their respective topographic forcing are poorly understood.

[8] In this study, the hydrographic measurements in the NSCS during the upwelling season are analyzed to elucidate the characteristics of the IU process in the NSCS (section 2). A three-dimensional model is then employed to simulate the observed processes (section 3) and to dynamically interpolate the governing forcing mechanism (section 4).

2. Observational Study

[9] Results obtained from hydrographic measurements in the NSCS during cruises in July and August 2000 and 2002 are shown in Figures 2 and 3. Five conductivity-temperature-depth (CTD) transects were sampled on the eastern part of the widened shelf in 2000 and eight transects covering the region from the Pearl River Estuary to east of the Taiwan Shoals were measured in 2002. The concomitant wind stress obtained from QuickScat and the sea surface temperature (SST) from MODIS averaged over the cruise periods are shown in Figure 4.

2.1. Horizontal Variability

[10] Forced by a strong southwesterly monsoon during the 2000 cruise (Figure 4), cold waters from the coastal upwelling were generally observed in the coastal region shoreward of the 50 m isobath. The intensity of the upwelling strongly varied alongshore and an IU existed

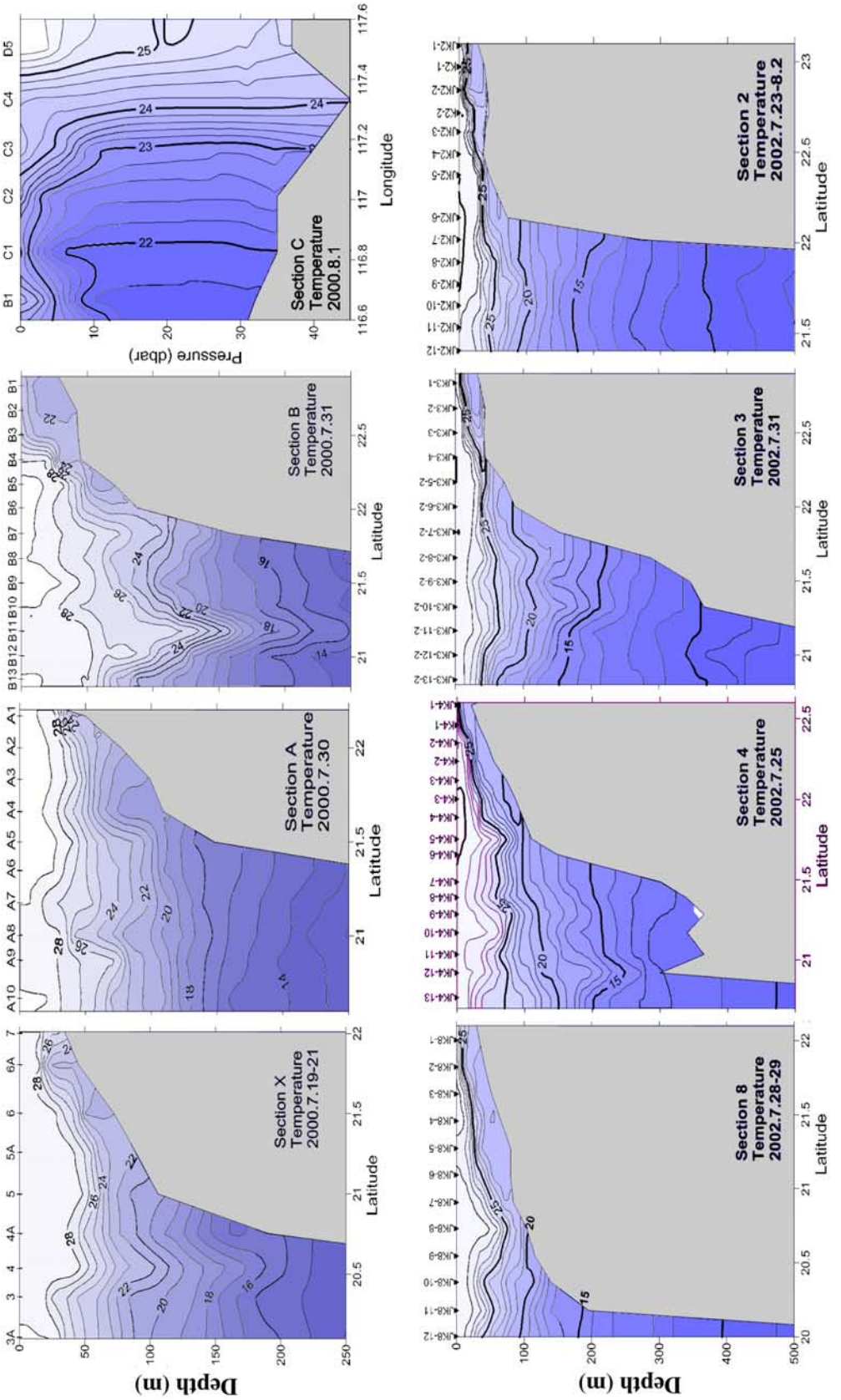

Figure 3. Across-shore sections of temperature (°C) along transects during summer cruises in (top) 2000 and (bottom) 2002.

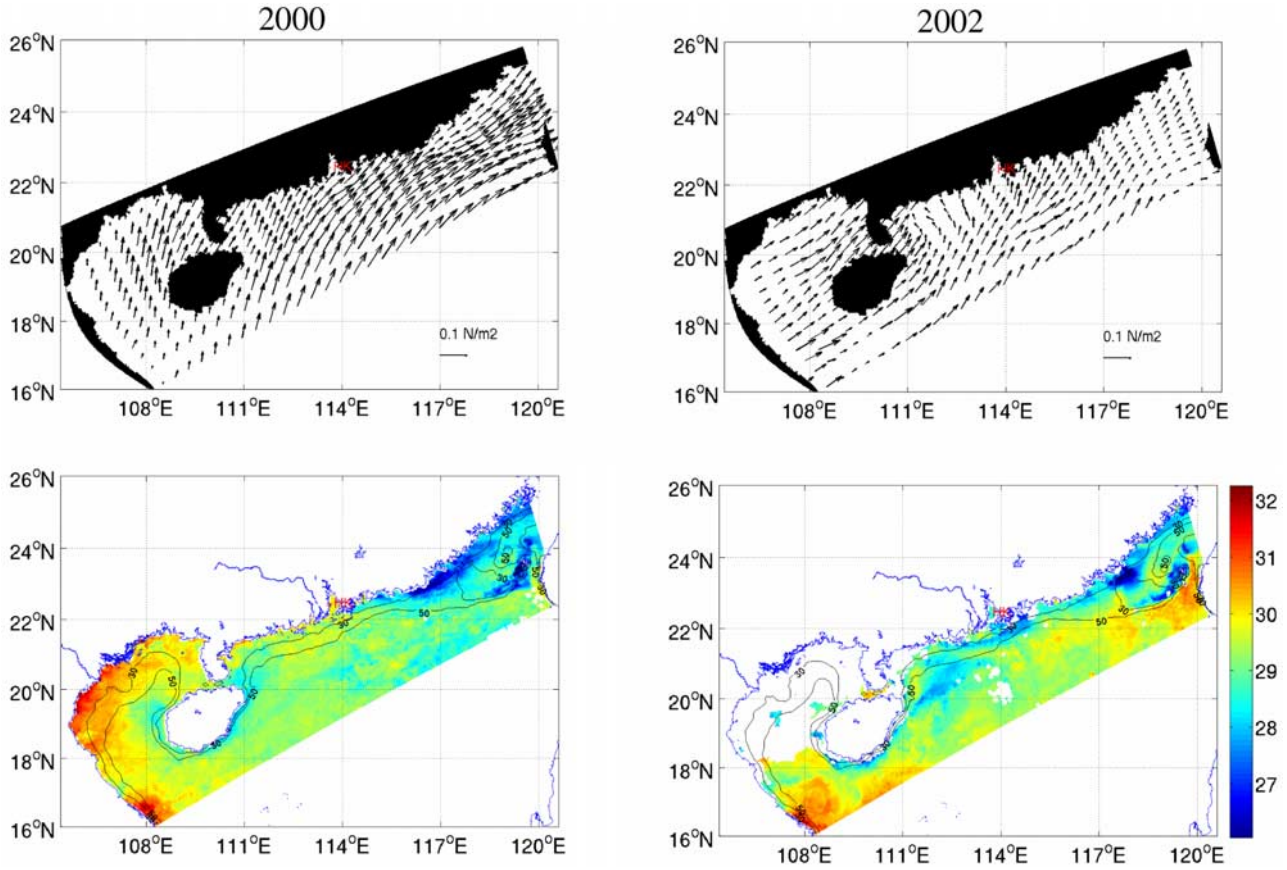

Figure 4. Vectors of QuickScat wind stress (Pa) and MODIS SST (°C) averages over the respective cruise periods in 2000 and 2002.

over the widened shelf (Figures 2 and 4). The maximum upwelling with the coldest water cooler than 23°C was centered off Shantou and expanded in both the alongshore and offshore directions.

[11] During the 2002 cruise, the southwesterly monsoon was relatively weak and gradually decreased eastward in the coastal waters (Figure 4). Analogous to the condition in 2000, the upwelling varied along the shelf (Figures 2 and 3) and the SST field from MODIS indicated the existence of an IU over the widened shelf. However, the water temperature averaged from the CTD tracks taken on different days showed a much stronger upwelling center near Shanwei (Figure 2b) instead of near Shantou as in 2000. During the survey from 22 July to 2 August, wind forcing in the NSCS was favorable to upwelling before 26 July; it turned shoreward between 27 and 29 July and southwestward afterward when a tropical cyclone approached the Taiwan Strait. The measurement of Shanwei transect was conducted on 25 July during the upwelling. The cold upwelled water at Shanwei was prohibited to advect toward Shantou where upwelling was greatly weakened because of the absence of the southwesterly wind after 26 July. In fact, as demonstrated in this study, this cold water near Shanwei is explained by the locally amplified shoreward cross-isobath transport near the head of the widened shelf, which could have been advected downstream and upwelled at the lee of the coastal cape near Shantou if southwesterly winds were prevailing over the entire NSCS.

2.2. Vertical Structures

[12] In the cross-shelf sections along lines X, A and B during 2000 (Figure 2a), the cold waters from depths up to 100 m were advected upward and shoreward over the slope of the shelf (Figure 3). Along line X, the isotherms near the coast tilted downward as the upwelling-favorable winds relaxed during the sampling period (20 July). However, the shoreward advance of the isotherms was still present in the bottom layer over the slope shoreward from the 100 m isobath. The upsloping cold water advection identified by the strong cold water tongue at 100 m near the shelf edge of line A (also see Figure 2a) reflected a shoreward invasion of deep water through the shoreward convex isobaths at the head of the widened shelf (Figure 1). The convex isobaths provide a short excursion for the deep colder waters to be directly carried toward the inner shelf. On the basis of this and the fact that the 22°C waters nearshore in B were not connected with the water mass of the same characteristics in deeper waters of section B, but have the same characteristics as that at 60 m of section A upstream, we suggest that the cold coastal waters off Shantou near B were likely to have originated upstream near the convex isobaths and subsequently advected eastward and shoreward downstream. This deep cold water mixed vigorously below the surface near line C (Figure 3) as it shoaled near Shantou. We noticed that there was an anticyclonic eddy in the water deeper than 500 m at line B. By examining the surface geostrophic current produced by the French Archiving, Validation, and

Interpolation of Satellite Oceanographic data (AVISO) with 1/3 degree resolution [*Rio and Hernandez*, 2004], we found that the eddy was associated with the intrusive slope current near the Dongsha Islands and stationed over the outer shelf offshore. Since it is away from the source of upsloping cold waters, the eddy's effect on the cross-shelf upwelling process nearshore is expected to be small.

[13] In 2002, the upward and shoreward tilting of the isotherms occurred along line 8 (Figure 2b) near the entrance of the Pearl River Estuary and along line 4 across the convex isobaths (Figure 3). Similar to the conditions in 2000, the cold waters were advected mainly from depths up to 100 m over the middle shelf. Despite the absence of cold water at the surface off Shantou, 22°C waters were found below the surface shoreward of the 50 m isobath along lines 2 and 3. Since there was no clear evidence to suggest that these cold waters were advected shoreward over the broad shelves along lines 2 and 3, their sources were conceivably from upstream.

[14] Although the measurements from both the hydrographic survey and remote sensing display characteristics of coastal upwelling with an IU over the widened shelf in the NSCS, the time and space dependence of the involved processes, which are necessary for a solid interpretation of the observed features, are absent in the spatially and temporally limited measurements. Thus, a three-dimensional model is utilized below to conduct a process-oriented simulation to understand the observed upwelling and the IU. The objective of this study is to identify the processes that create the observed IU and to understand the forcing mechanism for the IU in the NSCS.

3. Modeling Study

3.1. Ocean Model

[15] The ocean model used is the Regional Ocean Model System (ROMS) [*Shchepetkin and McWilliams*, 2005] for three-dimensional, time-dependent oceanographic flows governed by hydrostatic primitive equations. A local closure scheme based on the level-2.5 turbulent kinetic energy equations by *Mellor and Yamada* [1982] was adopted in the vertical mixing parameterization. The model domain extends from 15.99°N, 108.17°E in the southwest corner to about 25.81°N, 119.54°E in the northeast corner with its central axis directed 23° anticlockwise from true east (Figure 1). A curvilinear grid with a (450, 140) dimensional array was adopted as the horizontal coordinates (x, y) which form an average 3 km horizontal grid size. The stretched generalized terrain-following coordinate (s) [*Song and Haidvogel*, 1994] was adopted in the vertical coordinate. θ_s = 2.5 and θ_b = 0.8 were used in s, representing higher vertical resolution in the surface and bottom boundary layers, respectively, while avoiding artificial diffusion over the slope with a relatively large vertical grid spacing. The model has 30 vertical levels, which form the minimum and maximum grid spacing in the water column of less than 1 m over the inner shelf and about 10 m over the outer slope. The water depths, $h(x, y)$, were obtained by merging ETOPO2 (1/30°) from the National Geophysical Data Center (USA) with the water depths digitized from navigation maps published by the Maritime Safety Administration (China). The minimum water depth was set to 5 m and the topography was slightly smoothed to reduce truncation errors.

[16] We conducted a process study to investigate the isolated topographical effects on the coastal upwelling and IU in the NSCS. Thus, it was to our advantage to force the model with a spatially uniform southwesterly wind stress (0.025 Pa) representative of the upwelling conditions in the summer. It was equally sensible in this process-identified simulation to initialize the model with horizontally uniform temperature and salinity profiles obtained from field measurements at station 3A (Figure 1), which mirror climatological data in July (World Ocean Atlas 2001 [*Boyer et al.*, 2005]). The initial values of the velocities and surface elevation were set to zero. The model domain included two open boundaries in which open boundary conditions (OBCs) favorable to the wind-forced shelf circulation [*Gan and Allen*, 2005b; *Gan et al.*, 2005] were utilized on the eastern boundary while an oblique horizontal radiation condition [*Marchesiello et al.*, 2001] was applied on the southern boundary for two- and three-dimensional velocities, temperature and salinity. No-gradient condition was applied to the surface elevation in the open boundaries.

[17] In this study, the effects from nonlocal forcing due to the possible intrusion of the Kuroshio current was neglected so that the isolated topographic role of the upwelling can be identified. On the basis of evidences presented in section 2 and of the fact that our model result produces an IU similar to the observed features, the effect of nonlocal forcing on the IU over the middle and inner shelves is expected to be relatively small, particularly over the widened NSCS shelf during prevailing southwesterly winds. For the same reason, the buoyancy from the Pearl River discharge is neglected but included in a separated study [*Gan et al.*, 2009]. The buoyancy study reveals that enhanced stratification by the river plume thins the frictional layer of the surface and enhances the cross-shelf circulation in the upper water column such that the surface Ekman current and the compensating flow beneath the plume are amplified. Yet, the plume over the shelf has little effect on the intensity of the shoaling of the deep dense water.

3.2. Upwelling Flows

3.2.1. Response in Currents

[18] The general characteristics of the shelf flow responses to the wind-forced upwelling are shown by the surface and bottom velocities, the surface elevation and the magnitude of the depth-integrated velocity on day 30 in Figure 5. The density fields on days 10 and 30 are presented in Figure 6 to illustrate the evolution of the upwelling. Figure 5a shows a considerable alongshore variation in the upwelling coastal currents in the NSCS. Besides the jet off Hainan Island, the coastal currents flow mostly parallel to the coastline west of the Pearl River Estuary. The currents markedly veer offshore as they encounter the widened shelf near Shanwei and bifurcate into the northern and southern components near the Taiwan Shoals. The much stronger southern component flows southeastward following the isobaths at the outer edge of the widened shelf on the offshore side of the 50 m isobath, while the northern component moves northeastward and flows along the coast. Part of the northern component shifts southward after passing the Taiwan Shoals to rejoin the southern component. At the same time, the bottom

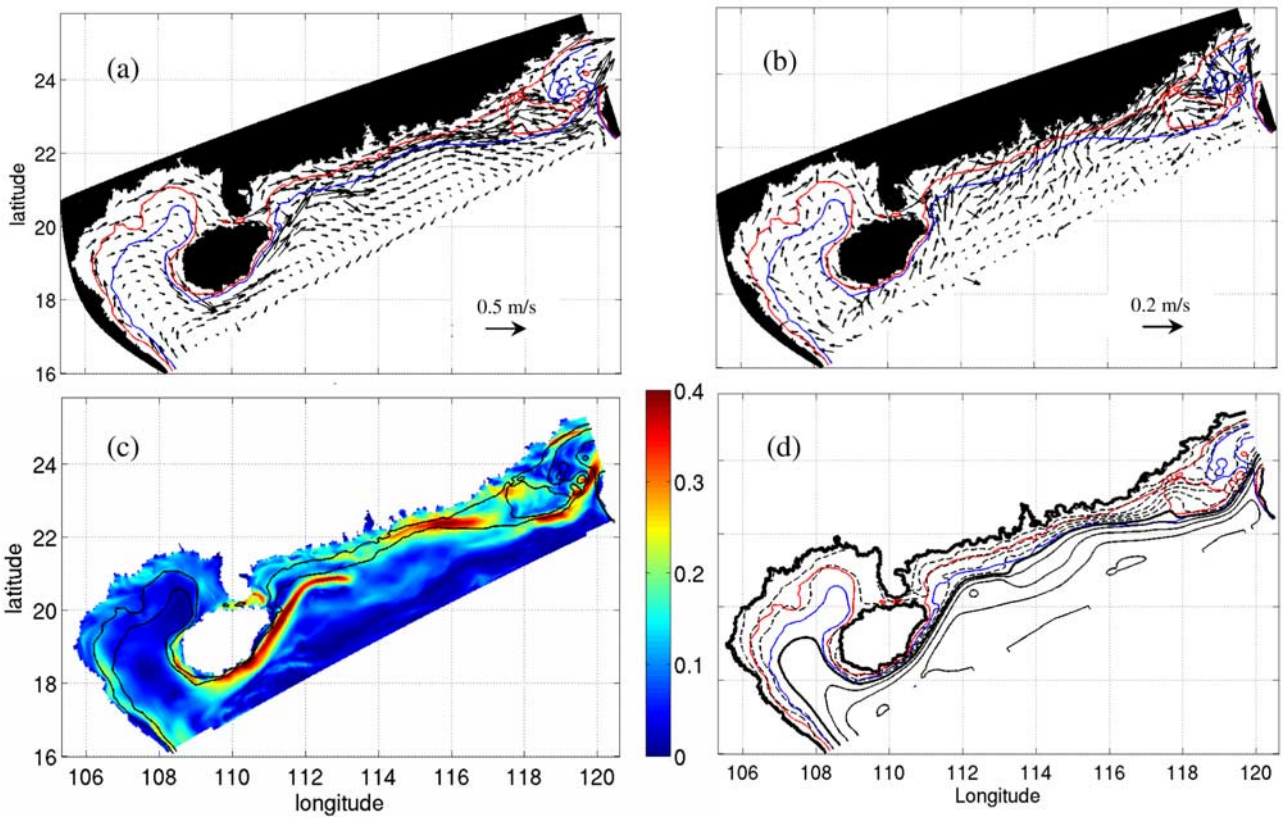

Figure 5. Daily mean (a) surface, (b) bottom velocity vectors (m s^{-1}), (c) depth-integrated velocity magnitude (m s^{-1}), and (d) surface elevation (m) on day 30. The contour interval for elevation is 0.02 m with the heavy contour line for 0 m. Dashed and solid contour lines refer to the negative and positive elevations, respectively. The 30 and 50 m isobaths are shown as red and blue contour lines, respectively.

currents over the shelf (Figure 5b) veer shoreward as a result of the Ekman balance between the bottom frictional stress and the Coriolis force. Relatively strong shoreward bottom transport occurs at the outer edge of the widened shelf crossing the 50 m isobath. The strongest shoreward currents, however, occur near the convex isobaths at the head of the widened shelf and subsequently flow shoreward and eastward toward Shantou.

[19] A strong depth-integrated velocity magnitude (Figure 5c) is found in a strip bounded by 30 m and 50 m isobaths at the convex isobaths. The intensification of the currents is also geostrophically correlated with the locally enhanced cross-shelf gradient of the surface elevation (η) (Figure 5d). The minimum value of η (<0) is found on the inshore side of the Taiwan Shoals where the maximum upwelling off Shanwei is located (Figures 2–4). The alongshore variation in η is evidently correlated with the alongshore variation of the isobaths, indicating the strong control by the bottom topography on the coastal currents.

3.2.2. Response in the Density Field

[20] The surface and bottom density fields on days 10 and 30 (Figure 6) show the evolution of the upwelling in response to the southwesterly winds. At the surface, relatively dense waters appear first in the inner shelf east of the Pearl River Estuary over the widened shelf on day 10. They extend offshore with increasing density from day 10 to day 30 and form the maximum upwelling center with the largest surface density near Shantou. The surface dense waters over the inner shelf are highly correlated with the shoreward and eastward advection at the bottom (Figure 5b). Relatively strong shoreward advance of the dense waters on the bottom occurs near the head of the widened shelf, which, with its amplified frictional bottom transport over the converging isobaths, allows the cold waters from depths to reach the inner shelf directly. There is a clear shoreward and northeastward density advection between the head and Shantou that transports the dense water toward Shantou from the head of the widened shelf.

[21] The simulated upwelling is qualitatively similar to the results obtained from the measurements (Figures 2–4). It shows the existences of an IU over the widened shelf with local maximum upwelling in the coastal waters off Shantou, and of an intensified shoreward dense water advection near the convex isobaths that supply the dense deep water downstream. Since the wind forcing is spatially uniform in the model, the upwelling features are conceivably associated with the variations in the shelf topography.

3.3. Cross-Shelf Structures

[22] The alongshore variations of the three-dimensional velocities (u, v) and density, ρ, on day 30 from a set of cross-shelf sections at different locations over the widened

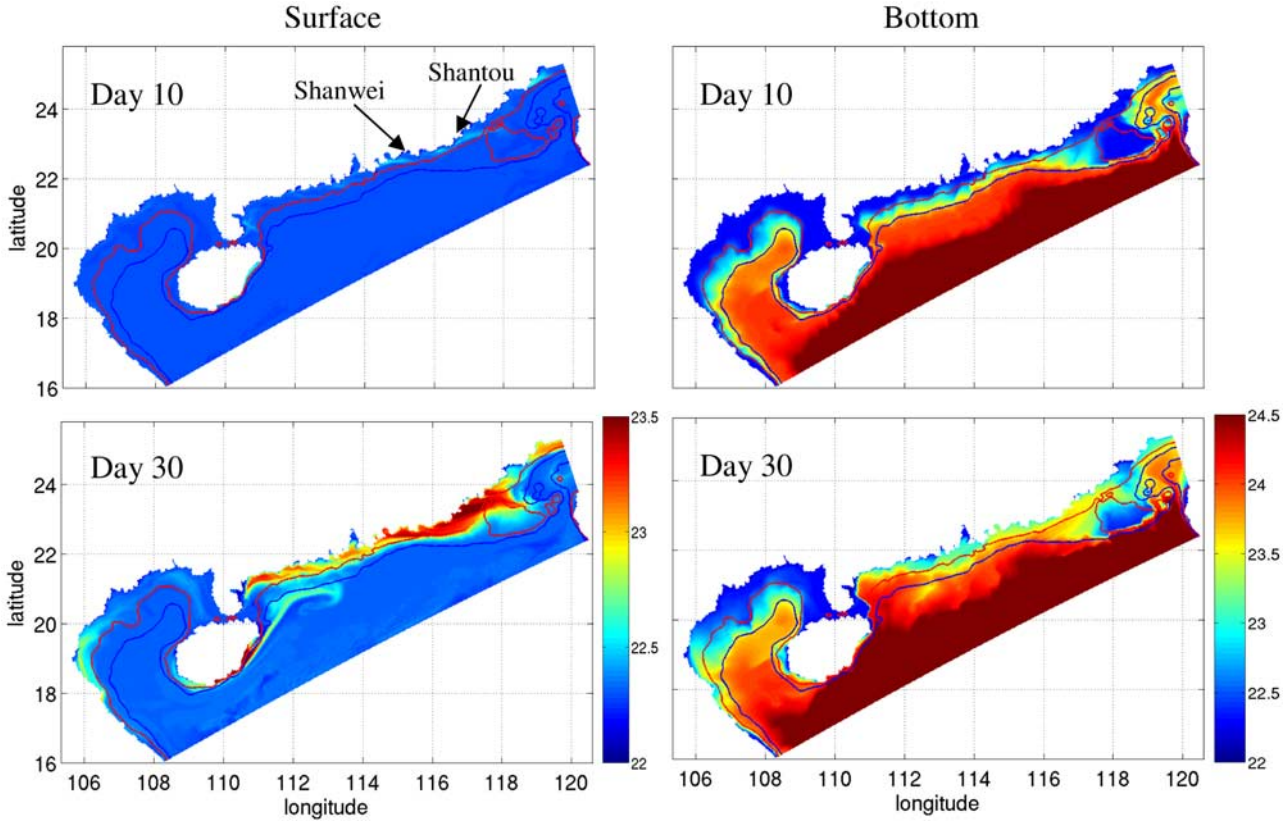

Figure 6. Daily average (left) surface and (right) bottom σ_θ (kg m^{-3}) on days 10 and 30, showing the strong shoreward advection near the convex isobaths at the head of the widened shelf and the subsequently eastward advection of dense bottom waters between Shanwei and Shantou during upwelling.

shelf, denoted by their alongshore grid numbers in Figure 1, are shown in Figure 7a. Since the model's curvilinear coordinate, *y*, is closely oriented to the direction normal to the coastline, *u* and *v* can be used to approximately represent the along-shelf and cross-shelf velocities, respectively. In particular, line 305, analogous to the survey lines A and 4 in Figures 2 and 3, and lines 338 and 372 cover the region of the maximum upwelling off Shanwei like survey lines B, 2 and 3. The density along section C is displayed in Figure 7b.

3.3.1. Alongshore and Cross-Shelf Velocities

[23] The fields of (*u*, *v*) show that the coastal upwelling jet intensifies near the convex isobaths, veers offshore from line 305 and bifurcates from line 338 toward line 378 (Figure 7a). The intensified *u* at 305, which centers about 30 km offshore and penetrates to the bottom, is induced largely by the confluence of currents over the local steepened shelf or converging isobaths at the head of the widened shelf (Figure 1). The jet subsequently bifurcates over the isobaths of the widened shelf, forming a southeastward current along the edge of the widened shelf and a weaker inshore component flowing eastward nearshore.

[24] The onshore currents occur largely at the bottom boundary layer. They generally reach larger values at water depths between 20 and 50 m. Along line 305, the near-bottom flow steers onshore in the bottom Ekman layer by the locally intensified *u*. The strongest positive *v*, which extends into the interior from the bottom boundary layer, occurs in the nearshore waters at line 338. At line 372, a positive *v* and an eastward *u* on the northern side of the Taiwan Shoals represent a northeastward current in the region, which, as described previously, is responsible for the downstream transport of the dense deep waters from the head of the widened shelf.

3.3.2. Cross-Shelf Density Advection

[25] In response to the current, shoreward advection of dense water over the slope occurs in the places where the positive cross shelf *v* is large (Figure 7a). The dense water is evidently advected shoreward toward the inner shelf from water up to 100 m deep at line 305. However, the dense water shoreward of the 50 m isobath at line 338 is not connected with the dense deep water farther offshore, similar to the observed results in Figure 2. The source of the nearshore dense water is evidently advected from upstream. Moreover, since the northern side of line 372 is blocked from the deeper water by the Taiwan Shoals, the local dense nearshore waters as well as the positive *v* is apparently associated with the cold waters advected by northeastward currents across the widened shelf from upstream, as also shown in Figure 5b, and is evidently the source of the densest waters in IU near Shantou. The density section along the east-west oriented line C (Figure 7b) further indicates an intrusion of cold water from the western part of the shelf and vertically strong mixing below the surface layer, similar to the measurements

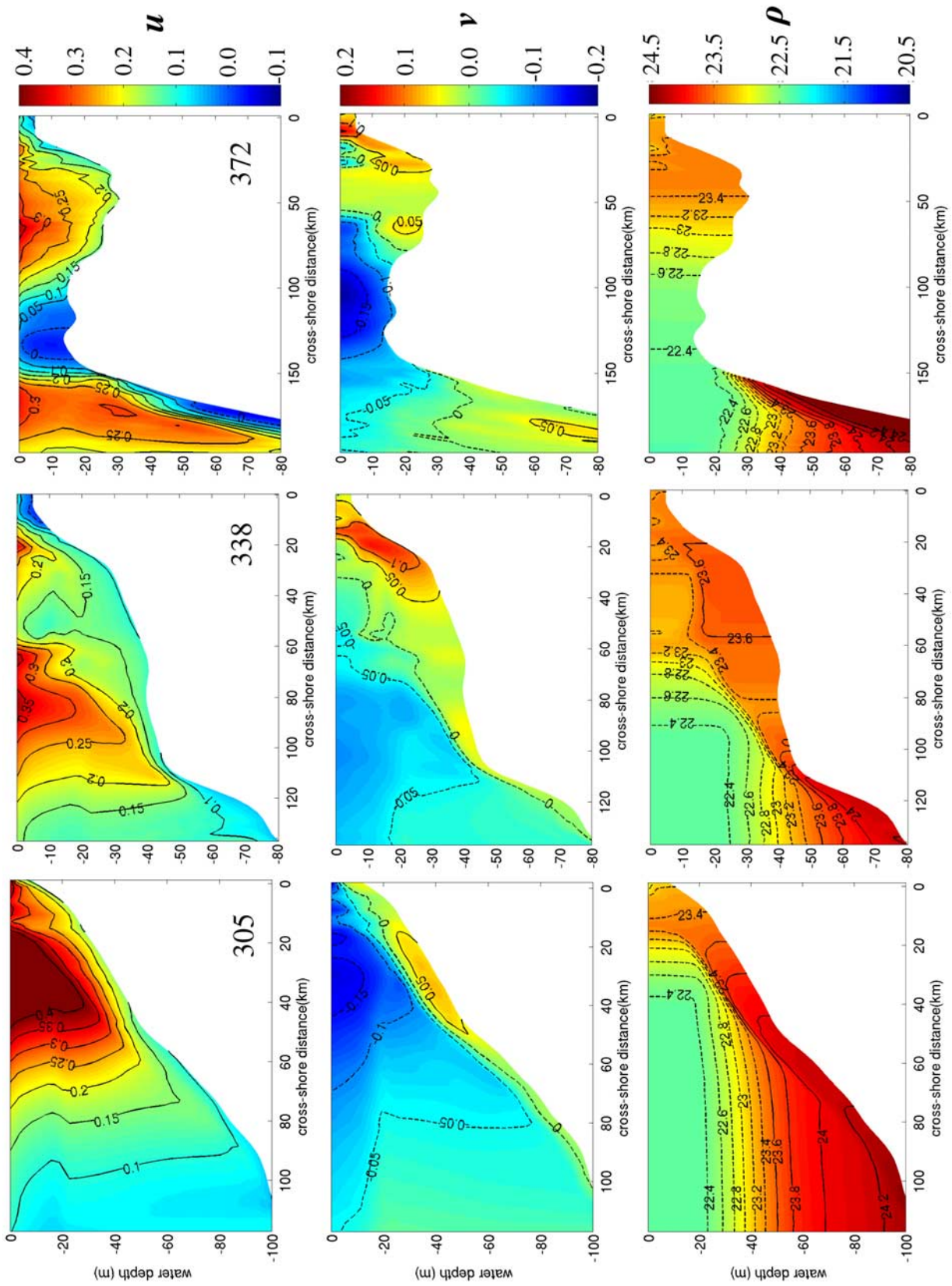

Figure 7a. Across-shore sections of daily averaged alongshore velocity, u (m s^{-1}); cross-shore velocity, v (m s^{-1}); and density, ρ (kg m^{-3}) at lines 305 (Shanwei), 338 (Shantou), and 372 (Taiwan Shoals) on day 30.

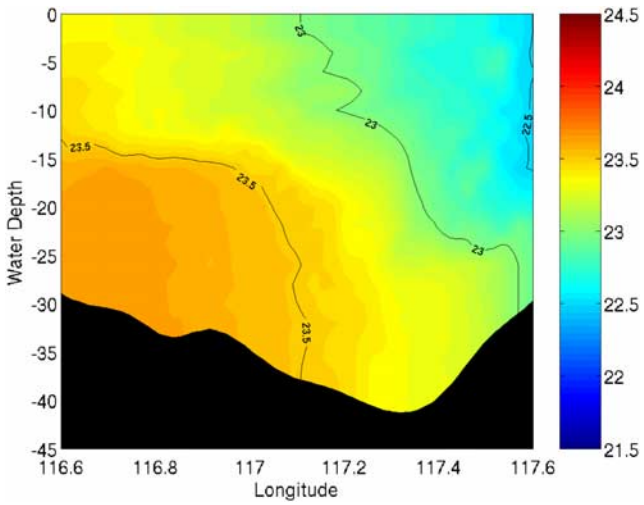

Figure 7b. Daily average σ_θ (kg m^{-3}) at the cross section along line C on day 30.

in Figure 3. The strong mixing is supposedly caused by the shoaling effect on the currents.

4. Analysis and Discussion

4.1. Alongshore Variation in Cross-Isobath Transport

[26] Since there is good evidence to link the IU with the forcing induced by the variable shelf topography in the widened shelf, it is useful to identify the alongshore conditions of the cross-isobath transport (Figure 8) and establish an understanding of the corresponding forcing mechanism (section 4.2). The methodology used to describe the transport across an isobath is given in Appendix A. According to the nature of wind-driven, cross-shelf circulation, the transport in a water column contains the upper and bottom boundary layers. With the vertical eddy viscosity, K_M, ranging from 10^{-3} m^2 s^{-2} to 6×10^{-3} m^2 s^{-2} near the surface and the bottom, obtained from the embedded turbulent model, the scale of the Ekman depth, $D_f = (2K_M/f)^{1/2}$, is estimated to be about 5–10 m. Here, f is the Coriolis parameter. On the basis of this and the fact that the relatively strong cross-isobath currents are mainly confined within 10 m in the

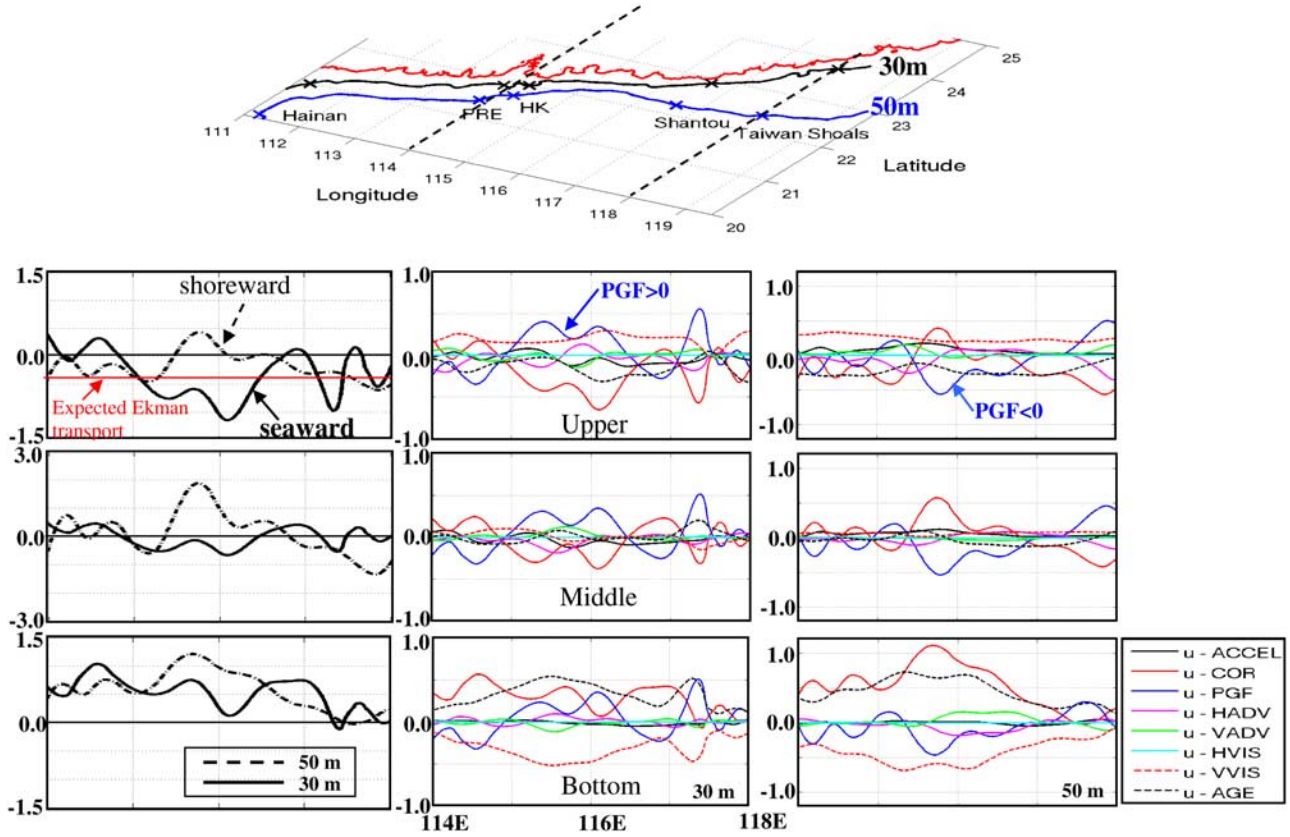

Figure 8. (left) Daily averaged mass fluxes (m^2 s^{-1}) cross the 30 m isobath (solid line) and the 50 m isobath (dashed line) on day 30. They are depth integrated for the upper 10 m (upper layer), middle 10 m for 30 m water depth and 30 m for 50 m water depth (middle layer), and bottom 10 m (bottom layer). Positive values of transport are directed shoreward. The surface Ekman transport (0.45 m^2 s^{-1}) is indicated by a thin red line. Daily average of terms from (1) along (middle) the 30 m and (right) the 50 m isobaths, which is depth integrated in the surface, middle, and bottom layers on day 30 (m s^{-2}). ACCEL, acceleration; COR, Coriolis force; PGF, pressure gradient force; HADV, horizontal nonlinear advection; VADV, vertical nonlinear advection; HVIS, horizontal viscous force; VVIS, vertical viscous force; AGE, ageostrophic term. All terms are multiplied by 10^5 except ACCEL which is multiplied by 10^6.

boundary layers (Figure 7a), the transport of the surface and bottom layers are chosen to be 10 m from the surface and bottom, respectively. The transport in the middle layer is then obtained in the water column between them. The positive (negative) value of transport refers to the shoreward (seaward) transport normal to the isobath. We focus on the region over the widened shelf where the IU occurs. The 30 m and 50 m isobaths are selected to represent the respective conditions over the inner and the middle shelves on the basis of the delineation in section 1 and condition in Figure 7a. The inner shelf is confined in the region shoreward of the 30 m isobath and its width increases from line 305 to line 338 as the shelf becomes wider. The inner shelf appears to occupy the entire water body north of the Taiwan Shoals where water is vertically homogeneous.

[27] As expected from the wind-driven upwelling, the surface and bottom Ekman transport are mainly directed seaward and shoreward, respectively. Considerably large magnitudes of cross-isobath transport also exist in the middle layer over both the inner and middle shelves (Figure 8). With the spatially uniform wind forcing of 0.025 Pa, the surface Ekman transport based on the infinite depth model, is estimated to be a constant value of $-\tau/\rho f = -0.45\ \mathrm{m^2\ s^{-1}}$, as shown by the red line in Figure 8. Evidently, the strong alongshore variation of the surface transport, and the similar variations in the middle and bottom layers, are formed by the sole variable forcing, the shelf topography. It is also clear that the transport in all layers is in phase, that is, the water column with a weak negative upper layer transport at a given location generally has a strong positive transport in the bottom and/or middle layers. The transport in the water column appears to be barotropic, but modified by the frictional currents in the surface and bottom layers.

[28] The alongshore variation of cross-isobath transport is highlighted by the existence of prominent transport across the inner and middle shelves over the widened shelf. In the upper layer along the 30 m isobath, the surface seaward transport is greatly amplified over the widened shelf with a peak value at 116°E and extending into the deeper layer. The shoreward transport mainly occurs in the bottom layer with two large values located at the convex isobaths near the head of the widened shelf and at the lee of Shantou, being separated by a small one near 116°E. Unlike the conditions that occur along the 30 m isobath, predominant shoreward transport exists along the 50 m isobath. A distinct peak shoreward transport occurs in the entire water column near the converging isobaths, and quickly decreases eastward away from the converging isobaths.

[29] The immediate conclusion that can be extracted from the characteristics of the cross-isobath transport is that the IU over the widened shelf is caused by the strengthened upslope cold advection from the deep water near the head of the outer widened shelf. This cold advection is strong, because the waters are transported from relatively cold deep water through the steep shelf at the head of the widened shelf. As to be shown below, the formation of a westward pressure gradient force here also contributes to the amplified shoreward transport in the water column. With the quickly developed upwelling circulation, the shoreward cold waters at Shanwei are advected eastward over the inner shelf by the strong upwelling current, before they can surface locally. These coldest waters over the inner shelf then upwell around Shantou where a coastal promontory locally intensifies upward motion [*Gan and Allen*, 2002]. On the basis of this, the cold center could occur in Shanwei if the northeastward upwelling coastal currents were weak on the eastern part of the NSCS, as in the case shown in Figure 2b. *Pringle* [2002] found the similar upwelling response over a widened shelf. From a barotropic, linear vorticity equation, he obtained the influential distance of widened shelf down wave as $L = (fh^2)/(Rr)$, where R and r are the bottom slope and linear bottom drag coefficient. Following this, the L in the NSCS is estimated to be 300 km, which is about twice of the distance from the head of the widened shelf at 115.5°E to 117°E where the amplified cross-isobath transport are felt (Figure 8). The deviation may arise from the barotropic approximation in the estimation.

[30] In contrast, no IU occurs in the region west of the widened shelf even though shoreward bottom transport exists there, mainly because of the absence of strong shoreward cold advection from the middle shelf like that provided by the widened shelf. The results here demonstrate the role of the interactive cross-shelf transport over the inner and middle shelves in wind-driven coastal upwelling.

4.2. Dynamics of Cross-Isobath Transport

[31] The forcing mechanism involved in the cross-isobath transport over the shelf is analyzed by the corresponding along-isobath momentum balances. The depth-dependent alongshore momentum equation in Cartesian coordinate system is written as

$$\overbrace{\frac{1}{D}\frac{\partial uD}{\partial t}}^{1} = -\frac{1}{D}\left[\overbrace{\left(\frac{\partial u^2 D}{\partial x}+\frac{\partial uvD}{\partial y}\right)}^{2}+\overbrace{\frac{\partial u\omega}{\partial \sigma}}^{3}+\overbrace{F_x}^{4}\right.$$
$$-\overbrace{fvD}^{5}-\overbrace{\frac{\partial}{\partial\sigma}\left(\frac{K_M}{D}\frac{\partial u}{\partial\sigma}\right)}^{6}$$
$$\left.+\overbrace{gD\frac{\partial\eta}{\partial x}+\frac{gD^2}{\rho_0}\int_\sigma^0\left(D\frac{\partial\rho'}{\partial x}-\frac{\sigma'}{D}\frac{\partial D}{\partial x}\frac{\partial\rho'}{\partial\sigma'}\right)d\sigma'}^{7}\right], \quad (1)$$

where ω is the velocity normal to the s surfaces, and K_M is the vertical turbulent viscosity coefficient. Here ρ and ρ_o are the water density and reference density, respectively. η is the sea surface elevation and $D = h + \eta$. The terms in (1) are acceleration, ACCEL (term 1), horizontal nonlinear advection, *HADV* (term 2), vertical nonlinear advection, *VADV* (term 3), the horizontal viscous term, *HVIS* (term 4), the Coriolis force, *COR* (term 5), the vertical viscous term, *VVIS* (term 6) and the pressure gradient force, *PGF* (term 7). It is also convenient to consider the variable of the sum of the *COR* and *PGF*, which is referred to as the ageostrophic pressure gradient, *AGE*, in (2):

$$AGE = -\frac{1}{D}\left[-fvD+gD\frac{\partial\eta}{\partial x}+\frac{gD^2}{\rho_0}\int_\sigma^0\left(D\frac{\partial\rho'}{\partial x}-\frac{\sigma'}{D}\frac{\partial D}{\partial x}\frac{\partial\rho'}{\partial\sigma'}\right)d\sigma'\right]. \quad (2)$$

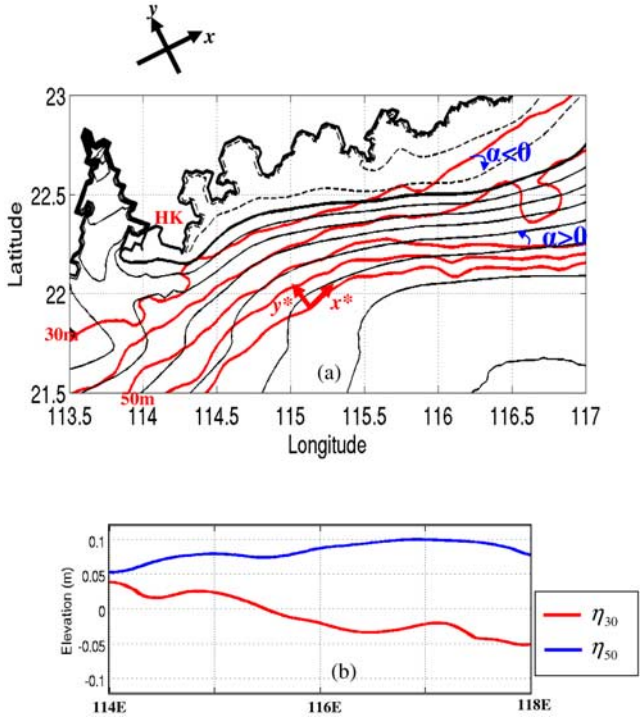

Figure 9. (a) Sea surface elevation (m) with positive values in solid black contours and negative values in dashed black contours. The isobaths of the 30, 40, 50, 60, and 70 m over EWS are shown by red contours. (b) Surface elevations along the 30 and 50 m isobaths.

[32] Since *AGE* is the net difference between the pressure gradient and the Coriolis force according to (2), the sign of *AGE* reflects the residual of the geostrophy either from the Coriolis force or from the pressure gradient. In the frictional boundary layers, *AGE* generally has the same sign as the Coriolis term and is balanced by the *VVIS*, representing the Ekman balance. To examine the forcing that drives the variable cross-isobath transport over the widened shelf, the terms in (1) are rotated to the along-isobath direction, x^*, and presented in Figure 8.

[33] Overall, the COR_x^*, which is proportional to the cross-isobath transport, is mainly balanced by the PGF_x^* in the middle layer, and by both the PGF_x^* and $VVIS_x^*$ in the upper and bottom layers according to

$$\int_{h_1}^{h_2} v_{y*}\,dz = \int_{h_1}^{h_2}\left[\frac{1}{\rho f}\frac{\partial p}{\partial x*} - \frac{VVIS_{x*}}{f}\right]dz = \int_{h_1}^{h_2}\left[-\frac{PGF_{x*}}{f} - \frac{VVIS_{x*}}{f}\right]dz, \quad (3)$$

where h_1 and h_2 ($h_2 > h_1$) are the water depths at the upper and lower limits of a given layer.

[34] The nonzero PGF_x^* is formed mainly by the deviation between the isobaths and isolines of η (Figure 9a) as a result of ageostrophy. The PGF_x^* geostrophically yields cross-isobath transport and is nearly barotropic and generally in phase with the same sign in the three layers. The Ekman flows, as indicated by the balance between AGE_x^* and $VVIS_x^*$, are significant in the upper and bottom layers. The magnitudes of $VVIS_x^*$ in the upper layer are determined by the intensity of the wind stress and local vertical mixing, while the $VVIS_x^*$ in the bottom boundary layer are highly correlated with the strength of the bottom velocity, u_x^*. The nonlinear advection terms are generally small in all layers and $HADV_x^*$ tends to balance $VADV_x^*$. Thus, the variation of the cross-isobath transport is controlled primarily by the variations in PGF_x^* and $VVIS_x^*$.

[35] The acceleration term is at least 10 times smaller than the other terms, but shows a relatively large spatial acceleration near the head of the widened shelf in the upper and middle layers and a deceleration or nonacceleration elsewhere, coherently reflecting the response of upwelling flow to the widened shelf.

[36] The across-isobath momentum balance (not shown) is much simpler and essentially geostrophic. The surface and bottom frictional transport (in the direction along the isobath) nearly balance each other. The across-isobath balance is related to the across-shelf transport by geostrophically forming a coastal jet that, in turn, produces the bottom across-isobath Ekman transport in the along isobath momentum equation.

4.2.1. Along-Isobath Pressure Gradient

[37] Along the 30 m isobath, PGF_{x*} becomes positive over the widened shelf and becomes negative near Shantou (Figure 8). The quasi-barotropic positive PGF_{x*} geostrophically strengthens/weakens the seaward/shoreward currents over the inner part of the widened shelf. The positive PGF_{x*} is formed as a result of a large negative angle, α, between the isobaths and isolines of η, or a strong negative $\partial\eta/\partial x^*$ (Figures 9a and 9b). In contrast, PGF_{x*} is mainly negative along the 50 m isobath over the middle part of the widened shelf. The peak value of the negative PGF_{x*} occurs where the 50 m isobath abruptly turns seaward near the head of the widened shelf. The alongshore variations of the PGF_{x*} in both the inner and middle shelves are well correlated with their concomitant transport variations, evidently indicating their important roles in the cross-shelf upwelling circulation.

[38] The significant alongshore variation of PGF_{x*} is largely associated with the shelf topography. Downstream of the convex isobaths, η drastically decreases along the 30 m isobath from 115°E toward the northeast region east of 116.6°E before it is increased farther downstream (Figure 9b). The alongshore variation of η over the inner shelf is strongly constrained by the variation of the coastline and the nearshore topography. According to *Gan and Allen* [2002], relatively low η is formed at the promontory of a coastal cape in order to acquire nonlinear centrifugal force, which generates negative/positive PGF_{x*} downstream/upstream of the coastal cape. Intensified upwelling was also found in the lees of coastal capes along the west Florida shelf [*Li and Weisberg*, 1999a]. As a result, two negative PGF_{x*} along the 30 m isobath are formed downstream of the coastal capes at Hong Kong and Shantou (Figures 8 and 9), while a positive one is formed between them.

[39] Yet, η keeps increasing along the southeastward veering 50 m isobath over the widened shelf and forms the westward (negative) PGF_{x*} or shoreward geostrophic currents. In fact, it can be shown that the net westward pressure gradient force over the widened shelf can be naturally produced by the net rate of the momentum change over the diverging isobaths. By integrating an inviscid,

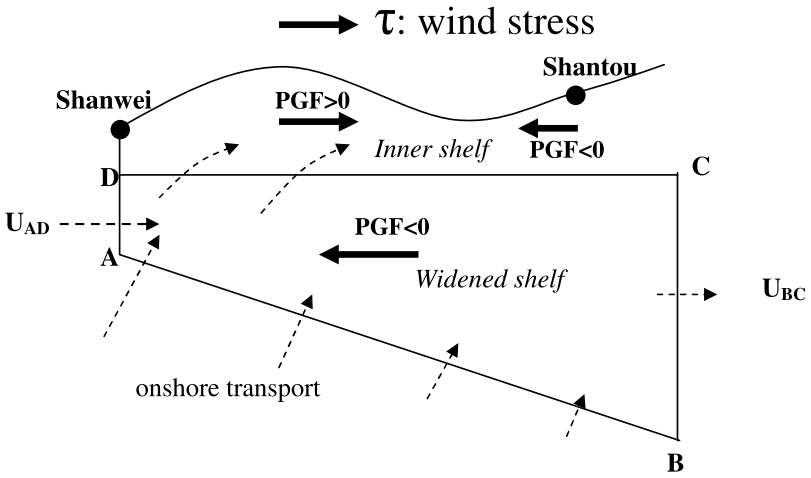

Figure 10. Schematic showing the wind-driven upwelling processes and forcing mechanism over the middle and inner shelves of a widened shelf.

steady momentum equation over a fixed volume, V [e.g., *Kundu and Cohen*, 2004], bounded with two streamlines, AB and CD, as well as with lines AD at the head of the widened shelf and BC downstream of it (Figure 10) normal to the respective mean velocities u_{AD} and u_{BC}, it can be proved that the net force, F, over the surface of V is

$$-\int_V \frac{\partial p}{\partial x^*} dV = F = \rho s_{BC} u_{BC}^2 - \rho s_{AD} u_{AD}^2, \tag{4}$$

where s_{AD} and s_{BC} are the areas at the cross sections along lines AD and BC, respectively. The right-hand side of (4) represents the net rate of the momentum change over V bounded by ABCD. With mass conservation, $u_{BC}s_{BC} = u_{AD}s_{AD}$, $F = \rho u_{BC}s_{BC}(u_{BC} - u_{AD})$. Since $u_{AD} > u_{BC}$ according to Figure 5c, the net westward force, $F<0$, is formed over the widened shelf as a result of the net rate of momentum influx within V. With the effect of the Earth's rotation, this net westward force forms the shoreward transport. The analysis demonstrates that the quasi-barotropic pressure gradient can be formed over the widened shelf. A similar net force was also found over a widened shelf off the Oregon coast during the upwelling season [*Gan and Allen*, 2005a]. Evidently, a larger difference in $(u_{BC}-u_{AD})$ over a sharper diverging part of the widened shelf is expected to have a larger F, similar to the argument presented by *Weisberg et al.* [2001] that a spatially accelerating jet during upwelling is needed to balance the overcompensated low layer transport due to the along-shelf pressure gradient.

4.2.2. Ekman Transport in the Boundary Layers

[40] Besides the cross-isobath transport that is geostrophically driven by the topographically induced PGF_{x*}, the cross-isobath circulation in the surface and bottom boundary layers largely defines the characteristics of the coastal upwelling (Figure 8). Since the wind stress is spatially uniform, positive $VVIS_x$* in the upper layer has little alongshore variation along both isobaths except north of the Taiwan Shoals where strong mixing occurs (Figures 3 and 7b). Thus, the alongshore variation of the cross-isobath transport in the upper layer is primarily modulated by the variation in PGF_{x*}. A quite different condition occurs in the bottom boundary layer. As the isobaths are converging toward the convex isobaths at the head of the widened shelf from the west, the upwelling jet spatially accelerates from the upstream toward the head and locally enhances the shoreward bottom Ekman transport, similar to the finding of *Oke and Middleton* [2000] and *Weisberg et al.* [2000]. Our results here also agree in principle with the finding of *Pringle* [2002] based on the linear, barotropic vorticity equation, except that the increasing bottom frictional effect near the head of the widened shelf may have been magnified through the water column. With the existence of quasi-barotropic PGF_{x*}, the net shoreward Ekman transport in the bottom layer is weakened by the mainly positive PGF_{x*} over the inner widened shelf, but intensified by the negative PGF_{x*} over the middle shelf.

5. Conclusions

[41] Observational and modeling studies have been conducted to investigate the processes and forcing mechanism of IU over the continental shelf in the NSCS. Both observational and modeling studies conceivably show that the IU in the NSCS is strongly controlled by the topography of the widened shelf. The processes and forcing invoked can be schematically summarized in Figure 10. The IU over a widened shelf is a phenomenon that may occur in many coastal oceans around the world, and the processes invoked generally include the geostrophically amplified shoreward advection of dense deep waters over the widened shelf, strong and efficient upslope dense water advection in the bottom boundary layer by the converging isobaths at the head of the widened shelf, the exchange between the inner and middle shelves and the locally amplified upward motion by the coastline and topography constraint over the inner shelf.

[42] The intensified cross-isobath transport over the widened shelf in the NSCS is formed by the variations of topographically induced PGF_x* and $VVIS_x$* over the middle shelf. Owing to the net rate of the momentum influx over the widened shelf, a negative PGF_x* is naturally formed in the diverging isobaths over the widened shelf during the

upwelling. This quasi-barotropic pressure gradient geostrophically strengthens the shoreward transport in the water column. At the same time, the converging isobaths at the head of the widened shelf enhance the shoreward transport in the bottom boundary layer. These shoreward cold waters are subsequently advected downstream by the developed coastal current over the inner shelf. The spatially varied upward motion over the inner shelf is regulated by PGF_x*, which is formed mainly by the variable coastline and the nearshore bottom topography. In the NSCS, a positive PGF_x* upstream and a negative PGF_{x*} downstream of the coastal cape near Shantou over the inner shelf are chiefly induced by the formation of higher pressure at the shoreward convex coastline. As a result, the cold dense waters advected from upstream near the head of the widened shelf outcrops at the lee of coastal cape near Shantou.

[43] This study demonstrates that a wind-driven coastal upwelling is controlled by the interactive processes over the inner and middle shelves that are largely influenced by the variation of shelf topography.

Appendix A: Derivation of Cross-Isobath Transport

[44] To resolve the model variables on a isobath, h_0, of the bottom topography, the variables in the model grid are first interpolated to a refined grid with a uniform resolution of 0.01 degree (about 1 km). The coordinates of h_0 in the domain are derived on the basis of water depths at four edges of the refined grid cells, assuming that isobath h_0 does not cross a grid cell twice. The angle between the tangential directions of the isobath and the direction of true east (i.e., the slope of the isobath (Figure A1)) is calculated by

$$\tan\theta_k = \frac{\delta y_k}{\delta x_k}, -\frac{\pi}{2} \le \theta_k \le \frac{\pi}{2}, \tag{A1}$$

where k is the grid number along the isobath, and δx_k and δy_k are defined as

$$\delta x_k = R(\lambda_{k+1} - \lambda_k)\cos\phi_k \tag{A2}$$

and

$$\delta y_k = R(\phi_{k+1} - \phi_k), \tag{A3}$$

respectively, where R is the radius of the Earth, $\lambda_{k+1} - \lambda_k$ is the longitude difference and $\phi_{k+1} - \phi_k$ is the latitude difference between the ascending contour points. The velocity normal to the isobath h_0 is then

$$v_y* = v_0\cos\theta - u_0\sin\theta, \tag{A4}$$

where u_0 is the eastward current and v_0 is the northward current. The cross-isobath mass transport per unit meter is

$$M_y* = \int_h^\eta v_y*(z)dz. \tag{A5}$$

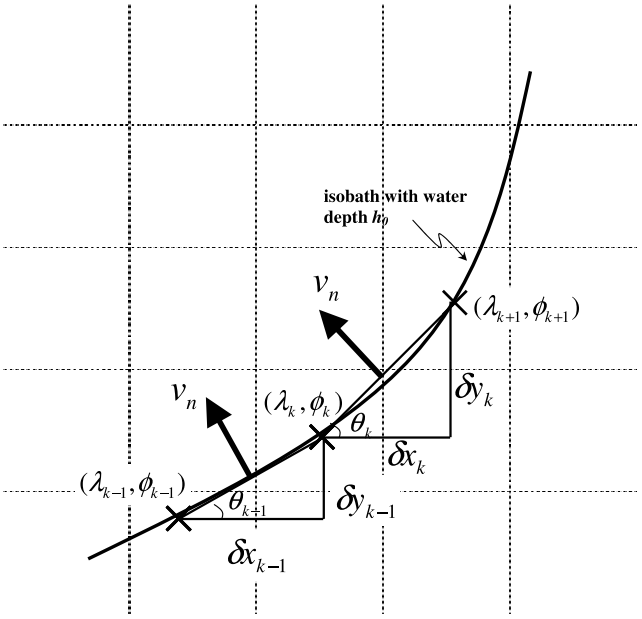

Figure A1. Interpolation scheme to calculate the velocity normal to an isobath h_0.

[45] **Acknowledgments.** This research project was supported by the National Key Basic Research Development Program 2009CB421208 and the Research Grants Council of Hong Kong under grants CERG-601105 and CERG-601204. We are grateful for the suggestions provided by the editor, associate editor, and reviewers that led to many improvements in the paper. Assistance in data processing by T. Zu and L. Liang is appreciated.

References

Allen, J. S., P. A. Newberger, and J. Federiuk (1995), Upwelling circulation on the Oregon continental shelf. Part 1: Response to idealized forcing, *J. Phys. Oceanogr.*, *25*, 1843–1866.

Austin, J. A., and S. J. Lentz (2002), The inner shelf response to wind-driven upwelling and downwelling, *J. Phys. Oceanogr.*, *32*, 2171–2193.

Barth, J. A., S. D. Pierce, and R. M. Castelao (2005), Time-dependent, wind-driven flow over a shallow midshelf submarine bank, *J. Geophys. Res.*, *110*, C10S05, doi:10.1029/2004JC002761.

Boyer, T. P., S. Levitus, J. I. Antonov, R. A. Locarnini, and H. E. Garcia (2005), Linear trends in salinity for the world ocean, 1955–1998, *Geophys. Res. Lett.*, *32*, L01604, doi:10.1029/2004GL021791.

Gan, J., and J. S. Allen (2002), A modeling study of shelf circulation off northern California in the region of the Coastal Ocean Dynamics Experiment: Response to relaxation of upwelling winds, *J. Geophys. Res.*, *107*(C9), 3123, doi:10.1029/2000JC000768.

Gan, J., and J. S. Allen (2005a), Modeling upwelling circulation off the Oregon coast, *J. Geophys. Res.*, *110*, C10S07, doi:10.1029/2004JC002692.

Gan, J., and J. S. Allen (2005b), On open boundary conditions for a limited-area coastal model off Oregon. Part 1: Response to idealized wind forcing, *Ocean Modell.*, *8*, 115–133, doi:10.1016/j.ocemod.2003.12.006.

Gan, J., J. S. Allen, and R. M. Samelson (2005), On open boundary conditions for a limited-area coastal model off Oregon. Part 2: Response to wind forcing from a regional mesoscale atmospheric model, *Ocean Modell.*, *8*, 155–173, doi:10.1016/j.ocemod.2003.12.007.

Gan, J., L. Li, D. Wang, and X. Guo (2009), Interaction of a river plume with coastal upwelling in the northeastern South China Sea, *Cont. Shelf Res.*, *29*, 728–740, doi:10.1016/j.csr.2008.12.002.

Han, W. Y., and K. M. Ma (1988), A study of coastal upwelling off eastern Guangdong (in Chinese), *Acta Oceanol. Sin.*, *10*(1), 52–59.

Janowitz, G. S., and L. J. Pietrafesa (1982), The effects of alongshore variation in bottom topography on a boundary current—(Topographically induced upwelling), *Cont. Shelf Res.*, *1*, 123–141.

Kosro, P. M. (2005), On the spatial structure of coastal circulation off Newport, Oregon, during spring and summer 2001 in a region of varying shelf width, *J. Geophys. Res.*, *110*, C10S06, doi:10.1029/2004JC002769.

Kundu, P. K., and I. M. Cohen (2004), *Fluid Mechanics*, 3rd ed., Elsevier, Amsterdam.

Lentz, S. J. (1995), Sensitivity of the inner-shelf circulation to the form of the eddy viscosity profile, *J. Phys. Oceanogr.*, *25*, 19–28.

Lentz, S., R. T. Guza, S. Elgar, F. Feddersen, and T. H. C. Herbers (1999), Momentum balances on the North Carolina inner shelf, *J. Geophys. Res.*, *104*, 18,205–18,226.

Li, L. (1993), Summer upwelling system over the northern continental shelf of the South China Sea: A physical description, in *Proceedings of the Symposium on the Physical and Chemical Oceanography of the China Seas*, edited by S. Jilan, W.-S. Chuang, and R. Hsueh, pp. 58–68, China Ocean, Beijing.

Li, Z., and R. H. Weisberg (1999a), West Florida shelf response to upwelling favorable wind forcing: Kinematics, *J. Geophys. Res.*, *104*, 13,507–13,527.

Li, Z., and R. H. Weisberg (1999b), West Florida continental shelf response to upwelling favorable wind forcing: 2. Dynamics, *J. Geophys. Res.*, *104*, 23,427–23,442.

Marchesiello, P., J. C. McWilliams, and A. Shclepetkin (2001), Open boundary conditions for long-term integration of regional oceanic models, *Ocean Modell.*, *3*, 1–20.

Mellor, G. L., and T. Yamada (1982), Development of a turbulence closure model for geophysical fluid problems, *Rev. Geophys.*, *20*, 851–875.

Mitchum, G. T., and A. J. Clarke (1986), The frictional nearshore response to forcing by synoptic scale winds, *J. Phys. Oceanogr.*, *16*, 934–946.

Oke, P., and J. Middleton (2000), Topographically induced upwelling off eastern Australia, *J. Phys. Oceanogr.*, *30*, 512–531.

Pringle, J. (2002), Enhancement of wind-driven upwelling and downwelling by alongshore bathymetric variability, *J. Phys. Oceanogr.*, *32*, 3101–3112.

Rio, M.-H., and F. Hernandez (2004), A mean dynamic topography computed over the world ocean from altimetry, in situ measurements, and a geoid model, *J. Geophys. Res.*, *109*, C12032, doi:10.1029/2003JC002226.

Shchepetkin, A. F., and J. C. McWilliams (2005), The regional oceanic modeling system (ROMS): A split-explicit, free-surface, topography-following-coordinate oceanic model, *Ocean Modell.*, *9*, 347–404.

Song, Y., and D. Haidvogel (1994), A semi-implicit ocean circulation model using a generalized topography-following coordinate system, *J. Comput. Phys.*, *115*, 228–244.

Song, Y. T., D. B. Haidvogel, and S. M. Glenn (2001), Effects of topographic variability on the formation of upwelling centers off New Jersey: A theoretical model, *J. Geophys. Res.*, *106*, 9223–9240.

Weisberg, R. H., B. D. Black, and Z. Li (2000), An upwelling case study on Florida's west coast, *J. Geophys. Res.*, *105*, 11,459–11,469.

Weisberg, R. H., Z. Li, and F. Muller-Karger (2001), West Florida shelf response to local wind forcing: April 1998, *J. Geophys. Res.*, *106*, 31,239–31,262.

Weisberg, R. H., R. He, Y. Liu, and J. I. Virmani (2005), West Florida shelf circulation on synoptic, seasonal, and interannual time scales, in *Circulation in the Gulf of Mexico: Observations and Models*, *Geophys. Monogr. Ser.*, vol. 161, edited by W. Sturges and A. Lugo-Fernandez, pp. 325–347, AGU, Washington, D. C.

Wyrtki, K. (1961), Physical oceanography of the southeast Asian waters: Scientific results of marine investigations of the South China Sea and the Gulf of Thailand, *NAGA Rep. 2*, 195 pp., Scripps Inst. of Oceanogr., La Jolla, Calif.

Zeng, L. M. (1986), A preliminary analysis of indicators of offshore upwelling off eastern Guangdong (in Chinese), *Trop. Oceanol.*, *5*(1), 68–73.

A. Cheung and J. Gan, Department of Mathematics and Atmospheric, Marine and Coastal Environment Program, Hong Kong University of Science and Technology, Kowloon, Hong Kong. (magan@ust.hk)

X. Guo and L. Li, Third Institute of Oceanography, State Oceanic Administration, Xiamen, 361005, China.